Optics and Laser Technology 100 (2018) 332–341

Contents lists available at ScienceDirect

Optics and Laser Technology

journal homepage: www.elsevier.com/locate/optlastec

Full length article

Performance analysis of coherent free space optical communications with sequential pyramid wavefront sensor

Wei Liu [a], Kainan Yao [b], Lu Chen [b,c], Danian Huang [d,*], Jingtai Cao [b], Haijun Gu [a]

[a] College of Communication Engineering, Jilin University, 5372 Nanhu Road, Changchun, Jilin 130012, China
[b] Changchun Institute of Optics, Fine Mechanics and Physics, Chinese Academy of Sciences, 3888, Nanhu Road, Changchun 130033, China
[c] University of Chinese Academy of Sciences, Beijing 10049, China
[d] College of Geoexploration Science and Technology, Jilin University, 938, West Democracy Street, Changchun, Jilin 130026, China

ARTICLE INFO

Article history:
Received 28 October 2016
Accepted 18 September 2017
Available online 16 October 2017

Keywords:
Sequential pyramid wavefront sensor
Fiber optics and optical communications
Active or adaptive optics
Atmospheric turbulence
Coherent communications

ABSTRACT

Based-on the previous study on the theory of the sequential pyramid wavefront sensor (SPWFS), in this paper, the SPWFS is first applied to the coherent free space optical communications (FSOC) with more flexible spatial resolution and higher sensitivity than the Shack-Hartmann wavefront sensor, and with higher uniformity of intensity distribution and much simpler than the pyramid wavefront sensor. Then, the mixing efficiency (ME) and the bit error rate (BER) of the coherent FSOC are analyzed during the aberrations correction through numerical simulation with binary phase shift keying (BPSK) modulation. Finally, an experimental AO system based-on SPWFS is setup, and the experimental data is used to analyze the ME and BER of homodyne detection with BPSK modulation. The results show that the AO system based-on SPWFS can increase ME and decrease BER effectively. The conclusions of this paper provide a new method of wavefront sensing for designing the AO system for a coherent FSOC system.

1. Introduction

With higher spectral efficiencies and data rates, a greater ability to decrease both background and thermal noise, and more sensitive coherent receivers, the performance of the coherent detection scheme is better than that of the intensity modulation direct detection in the free space optical communication (FSOC) systems [1–4]. Unfortunately, the atmospheric turbulence greatly degrades the performance of the coherent FSOC links [5]. The effects of laser beam propagation through turbulent atmosphere such as wavefront distortion, scintillation, beam wandering and spreading will not only degrade the entrance efficiency of receiving antenna but also cause the mismatch of the field of signal beam and local oscillator [6].

Adaptive optics (AO) system is successfully used to compensate atmospheric turbulence in coherent FSOC [7,8]. And as the main components of AO system, wavefront sensor is attracting extensive attention [9]. Generally, the Shack–Hartmann wavefront sensor (SHWFS) is widely used as an effective wavefront sensor in coherent FSOC [10]. Belmonte paid attention to elucidate how the addition of AO to the transmitter or receiver can reduce the effects of atmospheric propagation and to quantify the improvement on the performance of optical communications systems regarding coherent detection [11,12]. Zuo investigated the bit error rate (BER) performance of FSOC links in weak non-Kolmogorov turbulence and showed that BER decreased sharply as more Zernike modes were corrected by AO. Considering the influence of both the amplitude fluctuation and spatial phase aberrations, the Zernike mode was accurate when the ratio of receiving aperture diameter D to the coherent length r0 (D/r0) was large enough [13,14]. Ming Li evaluated the performance of the coherent FSOC employing quadrature array phase-shift keying modulation over the maritime atmosphere with atmospheric turbulence compensated by AO system based-on SHWFS [15]. Chao Liu and Jian Huang analyzed the mixing efficiency (ME) and BER performance improvement of the coherent FSOC with AO system based-on SHWFS by numerical simulation and experimental data of a 1.8 m telescope with AO system based-on a 127-subaperture SHWFS, under different D/r0 [16–19]. However, SHWFS was so sensitive to laser scintillation that the performance was limited in coherent FSO system. The focal plane wavefront sensor solved this problem, it had higher power usage ratio, but it was much more time cost [20]. In 1996, the pyramid wavefront sensor (PWFS) was proposed by Ragazzoni [21], and it was high sensitive in closed-loop operation, good characteristics of variable gain, and adjustable sampling in real time [22]. The PWFS had higher sensitivity and flexibility of sampling over established SHWFS. However, PWFS is difficult to

* Corresponding author.
E-mail address: professordn@163.com (D. Huang).

https://doi.org/10.1016/j.optlastec.2017.09.030
0030-3992/

manufacture and expensive, and the PWFS has not been used for FSO system. The reflective pyramid sensor is proposed by Wang utilizing a reflective pyramid mirror instead of a refractive pyramid prism [23]. Its working principle was identical to that of the PWFS. In addition, four charge-coupled devices and four relay lenses were required in a reflective pyramid sensor. Sequential operation of the micromirror array could instead of PWFS to measure wavefront aberrations, which was proposed in our previous work [24,25]. And it offered some advantages. First, comparing with the SHWFS, the spatial resolution was arbitrary adjustment and the sensitivity is higher than the SHWFS; Second, the SPWFS utilized the one-fourth pixels of detection element to realize the same wavefront resolution as PWFS, which meant higher uniformity of sensitivity and lower cost, especially for the avalanche photon diode (APD) array receiver of the coherent FSOC system. Third, the design of relay system could be more simplified than PWFS. Forth, SPWFS had weaker diffraction effect and smoother light intensity distribution. Thus, the goal of this paper is to evaluate the performance improvement of the coherent FSOC system with the AO system based-on SPWFS.

In this paper, the sequential operation approach of PWFS (SPWFS) which proposed in our previous work is first used in coherent FSOC to measure the wavefront aberrations. And the ME and the BER are analyzed to evaluate the performance of the coherent FSO communication. The numerical simulation is used to verify the feasible of the SPWFS for the coherent FSOC, and the experimental system of the SPWFS is designed to evaluate the improvement of the coherent FSOC performance with the SPWFS.

2. System model

The schematic diagram of coherent FSO system with AO to compensate atmospheric turbulence is shown in Fig. 1 [3]. As transmitting terminal, the laser beam is modulated into laser carrier signal and transmited through atmospheric channel. At the receiving terminal, the laser carrier frequency is mixed with a laser signal from local oscillation (LO signal) to generate the intermediate frequency signal. Then, according to the intermediate frequency signal, proper demodulator is used in order to be processed by digital signal processor. However, during the transmitting through the atmospheric channel, the laser carrier signal is distorted by atmospheric turbulence, and its wavefront and amplitude are disturbed. Accordingly, atmospheric compensation is indispensable in the coherent FSO system. In this paper, we introduce the AO unit in the coherent FSO system which consists of the wavefront corrector, the wavefront controller and the wavefront sensor. Firstly, the wavefront sensor measures the wavefront aberrations of the laser carrier signal. Secondly, according to the measured aberrations, wavefront controller controls the wavefront corrector. Finally, the wavefront corrector corrects the wavefront aberrations in real time. Thus, atmospheric turbulence is compensated and the quality of the received laser carrier signal is improved.

3. Theoretical analysis

3.1. The theory of SPWFS

The basic configuration of the PWFS is shown in Fig. 2. It consists of three fundamental parts: a tip-tilt mirror conjugated to the pupil is used to modulation, a square-based glass pyramid with its vertex at the nominal focal plane of the system and a relay lens that forms four images of the exit pupil on a detector plane. Where the role of modulation is to increase the linearity and dynamic range of the sensor [21].

Fig. 2 shows that the pupil re-imager is used to form images of the pupil relayed by the four facets of the pyramid on the detector. For each beam, it can be seen as being masked 3 quadrants on the focus plane. The signal is computed for each sub-aperture with the following formula (similar to a quad-cell signal):

$$S_x(x,y) = \frac{[I_1(x,y) + I_4(x,y)] - [I_2(x,y) + I_3(x,y)]}{I_1(x,y) + I_2(x,y) + I_3(x,y) + I_4(x,y)} \quad (1)$$

$$S_y(x,y) = \frac{[I_1(x,y) + I_2(x,y)] - [I_3(x,y) + I_4(x,y)]}{I_1(x,y) + I_2(x,y) + I_3(x,y) + I_4(x,y)} \quad (2)$$

where $I_n(x,y)$ is the image intensity of the position (x,y) of the nth quartile. In the case of a circular tip-tilt modulation having amplitude bigger than the local tilt of the aberrated wavefront $w(x,y)$, geometrical optics calculations show that [21]:

$$\frac{\partial_w(x,y)}{\partial x} \propto \sin\left[\frac{\pi}{2} S_x(x,y)\right] \quad (3)$$

$$\frac{\partial_w(x,y)}{\partial y} \propto \sin\left[\frac{\pi}{2} S_y(x,y)\right] \quad (4)$$

The Eq. (3) and the Eq. (4) show that the local tilt of wavefront is in proportion to the output signal of the PWFS when the wavefront aberrations are low enough.

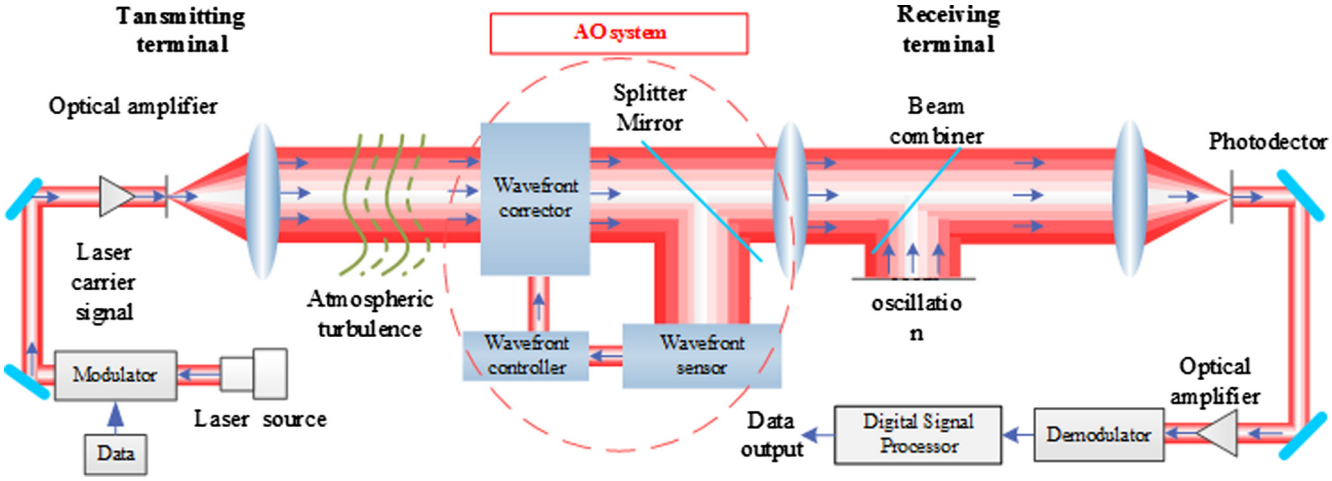

Fig. 1. The schematic diagram of FSO communication system.

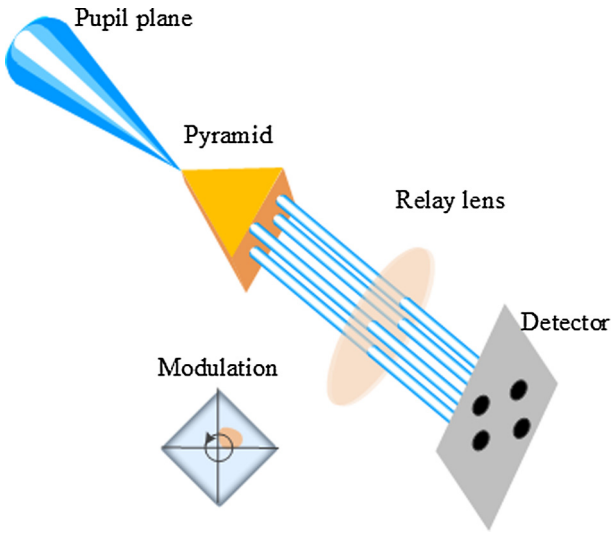

Fig. 2. The schematic diagram of the PWFS.

The schematic diagram of the SPWFS we proposed in our previous work is shown in Fig. 3 [24]. Thus, only the geometrical optics analysis is given in this paper.

A micro-mirror array which consists of 2×2 tip-tilt mirrors is placed on the focus plane as the replacement for the pyramid prism. If the micro-mirror is no tilt, all the light will be reflected onto the detection plane. The SPWFS divides one wavefront sensing procedure into four steps. In each step only one micro-mirror will be tilted at an angle. In other words, the light which comes from three quadrants will be detected and the remaining one quadrant will be discarded.

The output signal of the SPWFS can described as:

$$S'_x(x,y) = \frac{3 \times [(I_{s2}(x,y) + I_{s3}(x,y)) - (I_{s1}(x,y) + I_{s4}(x,y))]}{I_{s1}(x,y) + I_{s2}(x,y) + I_{s3}(x,y) + I_{s4}(x,y)} \quad (5)$$

$$S'_y(x,y) = \frac{3 \times [(I_{s3}(x,y) + I_{s4}(x,y)) - (I_{s1}(x,y) + I_{s2}(x,y))]}{I_{s1}(x,y) + I_{s2}(x,y) + I_{s3}(x,y) + I_{s4}(x,y)} \quad (6)$$

The Eq. (3) and the Eq. (4) are also true for the Eq. (5) and the Eq. (6) with an uncomplicated geometrical analysis. So it can be seen that the principle of SPWFS is equivalent to PWFS in geometrical optics analysis.

According to the geometrical optics model, since the sequential operation approach, the detection element of SPWFS only need to accommodate one pupil image instead of four pupil images with PWFS, which means no more than one-fourth optical size can realize the same wavefront resolution as PWFS [24,25].

Furthermore, based-on the analysis of diffraction theory in our previous work, the intensity of SPWFS on the detection plane is three times larger than that on each quadrant of the PWFS [24,25]. However, the light energy of diffraction effect of the SPWFS is similar to the PWFS, so less light energy will go out of detection pupil and the relative intensity fluctuation is smaller than the PWFS. Both will result in a higher light utilization than the PWFS.

3.2. Analysis of ME and BER in coherent FSOC

As mentioned, in coherent FSO system, the received laser carrier is mixed with LO signal, generate the intermediate frequency signal. The received laser carrier and the LO signal are given by [16]:

$$E_S = U_S(r,\varphi)cos[\omega_S t + \psi_S + \psi_S(r,\varphi)] \quad (7)$$

$$E_{LO} = U_{LO}(r,\varphi)cos[\omega_{LO} t + \psi_{LO} + \psi_{LO}(r,\varphi)] \quad (8)$$

where $U_S(r,\varphi)$ and $U_{LO}(r,\varphi)$ is the amplitude of laser carrier and LO signal. $\psi_S(r,\varphi)$ and $\psi_{LO}(r,\varphi)$ is the variable phase related to spatial position of laser carrier and LO signal, respectively. ω_S and ω_{LO} are their angular frequency, respectively. The current after frequency mixing is given by:

$$i = c \int_\sigma \eta(E_T \times H_T) ds \quad (9)$$

where H_T is the magnetic field distribution after frequency mixing, $E_T \times H_T$ is the Poynting vector, η is the quantum efficiency of the detector, and c is constant, σ is the area of the detector. Simply the Poynting vector, we can obtain:

$$E_T \times H_T = (E_S + E_{LO}) \times (H_S + H_{LO}) = E_S H_{LO} + E_{LO} H_S = 2\sqrt{\frac{e\varepsilon_0}{h\nu} E_S E_{LO}} \quad (10)$$

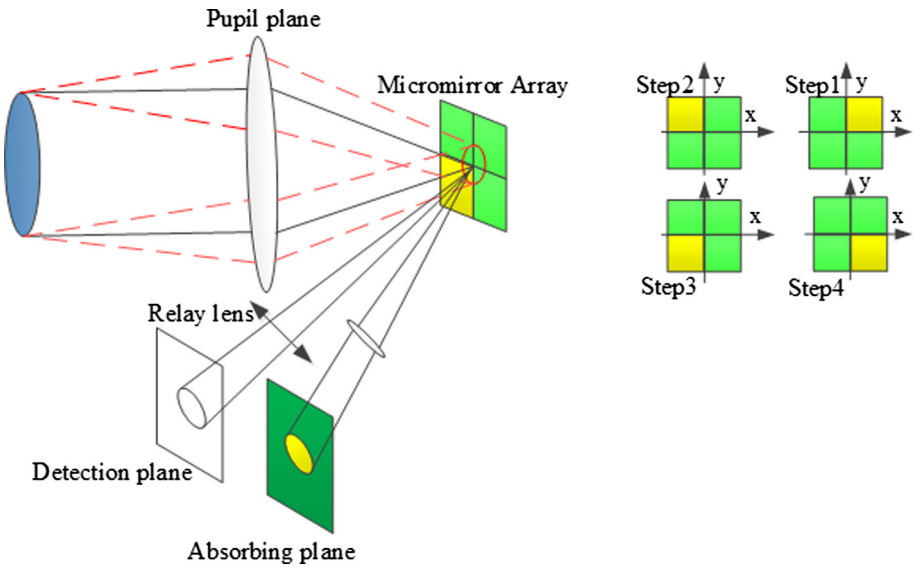

Fig. 3. Schematic diagram of SPWFS.

where e is electron charge, h is the Placnk constant, v is the frequency of the carrier signal, ε_0 is the permittivity of vacuum, H_S is the magnetic field distribution of the laser carrier, and H_{LO} is the magnetic field distribution of the LO signal. Take Eqs. (7), (8) and (10) into Eq. (9), the heterodyne intermediate frequency signal current is obtained:

$$\begin{aligned} i_h(t) &= \tfrac{ce\varepsilon_0\eta}{h\nu}\int_0^{2\pi}\int_0^{r_0} U_S(r,\varphi)U_{LO}(r,\varphi)\cos[\omega_{IF}t+\Delta\psi+\Delta\psi(r,\varphi)]rdrd\varphi \\ &= \tfrac{ce\varepsilon_0\eta}{h\nu}\{\cos(\omega_{IF}t)\int_0^{2\pi}\int_0^{r_0} U_S(r,\varphi)U_{LO}(r,\varphi)\cos[\Delta\psi+\Delta\psi(r,\varphi)] \\ &\quad -sin(\omega_{IF}t)\int_0^{2\pi}\int_0^{r_0} U_S(r,\varphi)U_{LO}(r,\varphi)\sin[\Delta\psi+\Delta\psi(r,\varphi)]\} \end{aligned} \tag{11}$$

where c is a constant. $\Delta\psi(r,\varphi)$ is the phase difference related to coordinate position. $\Delta\psi$ is the fixation phase difference irrelevant to coordinate the position. r_0 is the photosensitive surface of the detector. $\omega_{IF}=|\omega_S-\omega_{LO}|$ is the intermediate angular frequency, and when $\omega_{IF}=0$, it is called homodyne detection, and if $\omega_{IF}\neq 0$, it is called heterodyne detection. The mean square value of the intermediate frequency signal current is given by:

$$\langle i_h^2\rangle = \frac{1}{2}\left(\frac{ce\varepsilon_0\eta}{h\nu}\right)^2\left|\int_0^{2\pi}\int_0^{r_0} U_s(r,\varphi)U_{LO}(r,\varphi)\exp[i\Delta\psi(r,\varphi)]rdrd\varphi\right|^2 \tag{12}$$

For the intensity of the LO signal is much larger than the intensity of the laser carrier, the detector noise is mainly shot noise, so the mean square value of the noise current is given by [16]:

$$\langle i_N^2\rangle = 2eI_{LO}B = \left(\frac{c\varepsilon_0 e^2\eta}{h\nu}\right)B\int_0^{2\pi}\int_0^{r_0}[U_{LO}(r,\varphi)]^2rdrd\varphi \tag{13}$$

where I_{LO} is the direct current generated by LO signal, B is the noise bandwidth of the detector. The signal noise ratio (SNR) is defined by the ratio of the mean square value of the intermediate frequency signal current and the mean square value of the noise current:

$$\begin{aligned} SNR &= \frac{\langle i_h^2\rangle}{\langle i_N^2\rangle} \\ &= \left(\frac{\eta P_S}{h\nu B}\right)\frac{|\int_0^{2\pi}\int_0^{r_0} U_S(r,\varphi)U_{LO}(r,\varphi)\exp[i\Delta\psi(r,\varphi)]rdrd\varphi|^2}{\int_0^{2\pi}\int_0^{r_0}[U_{LO}(r,\varphi)]^2rdrd\varphi\int_0^{2\pi}\int_0^{r_0}[U_S(r,\varphi)]^2rdrd\varphi} \end{aligned} \tag{14}$$

where P_S is the laser signal power, which is expressed by:

$$P_S = \frac{c\varepsilon_0}{2}\int_0^{2\pi}\int_0^{r_0}[U_S(r,\varphi)]^2rdrd\varphi \tag{15}$$

In the coherent FSOC, the power of LO signal is large enough to the extremity of shot noise. Thus, the SNR of the coherent FSOC without atmospheric turbulence can reach to:

$$SNR_0 = \frac{\eta P_S}{h\nu B} \tag{16}$$

Comparing the Eq. (14) to the Eq. (16), we can obtain the ME of the heterodyne detection:

$$\gamma_h = \frac{|\int_0^{2\pi}\int_0^{r_0} U_S(r,\varphi)U_{LO}(r,\varphi)\exp[i\Delta\psi(r,\varphi)]rdrd\varphi|^2}{\int_0^{2\pi}\int_0^{r_0}[U_{LO}(r,\varphi)]^2rdrd\varphi\int_0^{2\pi}\int_0^{r_0}[U_S(r,\varphi)]^2rdrd\varphi} \tag{17}$$

Specially, when $\omega_{IF}=0$, under the condition of homodyne detection, we can obtain the current and the ME:

$$\begin{aligned} i_{zh}(t) &= \frac{e\varepsilon_0 c\eta}{h\nu}\int_0^{2\pi}\int_0^{r_0} U_S(r,\varphi)U_{LO}(r,\varphi)\cos[\Delta\psi \\ &\quad +\Delta\psi(r,\varphi)]rdrd\varphi \end{aligned} \tag{18}$$

$$\gamma_{zh} = \frac{|\int_0^{2\pi}\int_0^{r_0} U_S(r,\varphi)U_{LO}(r,\varphi)\cos[\Delta\psi(r,\varphi)]rdrd\varphi|^2}{\int_0^{2\pi}\int_0^{r_0}[U_{LO}(r,\varphi)]^2rdrd\varphi\int_0^{2\pi}\int_0^{r_0}[U_S(r,\varphi)]^2rdrd\varphi} \tag{19}$$

According to the Eqs. (17) and (19), the ME is defined by the ratio of the SNR with the atmospheric turbulence and the SNR without atmospheric turbulence. And it is related to both the amplitude of carrier signal and LO signal, and spatial phase distribution difference (SPDD). In this paper, assuming the signal carrier at the receiving terminal is the plane wave, and the LO signal is the plane wave with uniform intensity, the ME is influence by SPDD directly. The SPDD is smaller, the ME is larger. The AO system can decrease the SPDD between the carrier signal and the LO signal, then the ME is improved. In the ideal condition, ME can reach to 1, but limited by optical aperture and the waist radius of Gaussian beam in the real system, there is an extremum of ME which is below 1.

In the coherent detection system, the BER can be given by [16]:

$$BER = \frac{1}{2}erfc\left(\frac{Q}{\sqrt{2}}\right) \tag{20}$$

where $erfc$ is the complementary error function, $Q=\sqrt{SNR}$. For synchronous binary phase shift keying (BPSK) modulation, the optical power at the receiving terminal is expressed by:

$$P_S = N_P h\nu B \tag{21}$$

The SNR without atmospheric turbulence is given by:

$$SNR_0 = \frac{2\eta P_S}{h\nu B} = 2\eta N_P \tag{22}$$

where N_p is the number of photons received within a single bit [16]. For the BPSK modulation, the BER of the heterodyne detection is:

$$BER_h = \frac{1}{2}erfc\left(\sqrt{\eta N_P\gamma_h}\right) \tag{23}$$

Then, the BER of the homodyne detection is:

$$BER_{zh} = \frac{1}{2}erfc\left(\sqrt{2\eta N_P\gamma_{zh}}\right) \tag{24}$$

4. Numerical simulation

In our previous work, we verified the feasibility of SPWFS, and analyzed its performance from SNR, the noise equivalent angle and other aspects. The influence of SPWFS on coherent FSOC is analyzed in this paper. In the numerical simulation, the closed-loop control bandwidth, the noise of AO system and the isoplanatic errors are ignored. Assuming the amplitude distributions of the received optical signal and the LO laser are uniform, we focus on the impact of AO system based-on SPWFS on the SPDD. Under different atmospheric turbulence, firstly, ME and BER of coherent FSOC is analyzed with BPSK modulation during the aberrations correction of AO system based-on SPWFS. Then, the influence of N_p on BER is discussed. Finally, the BER of coherent FSOC with different modulation is analyzed.

The Zernike mode is the most common method to describe the wavefront phase distribution. The coefficients of the Zernike are generated by the method of the Zernike polynomials [26]. In this paper, the wavefront aberrations of the received optical signal and residual aberrations after the correction of AO system based-on SPWFS are also described by Zernike mode. We obtain the BER and ME of coherent FSOC during the aberrations correction of AO system based-on SPWFS by the Eqs. (17), (19), (23) and (24).

The D/r_0 is used to evaluate the turbulence size in the coherent FSOC. In the case of receiving antenna of the coherent FSOC system is usually less than 1 m, when $D/r_0<2$, it is weak turbulence, if $2<D/r_0<10$, the turbulence is medium, and it is strong turbulence when $D/r_0<10$ [16]. In order to analyze the influence of AO system based-on SPWFS on the performance of the coherent FSO, in the following numerical simulation, the influence of SPDD on the per-

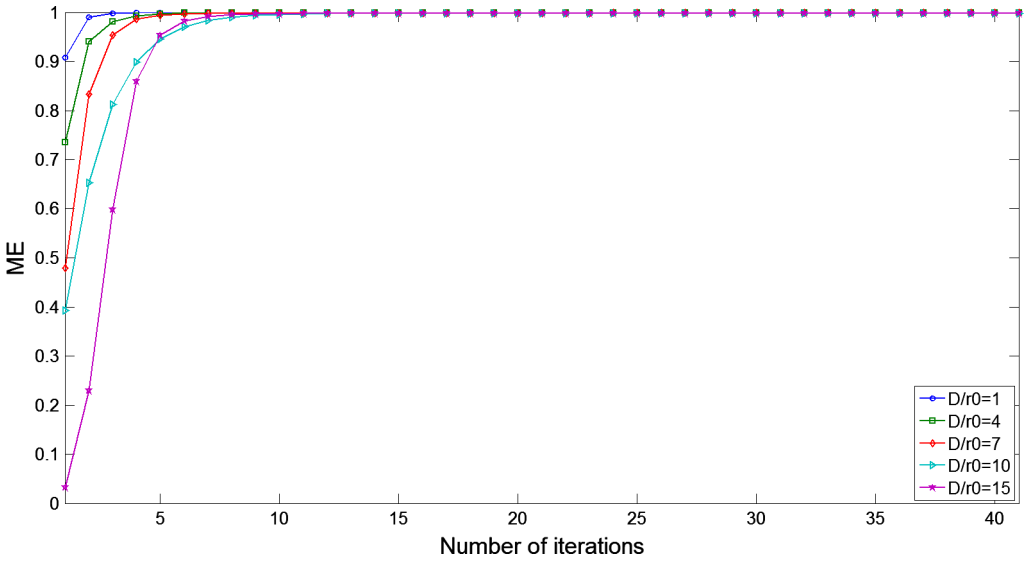

Fig. 4. The ME of homodyne detection during the aberrations correction based-on the SPWFS.

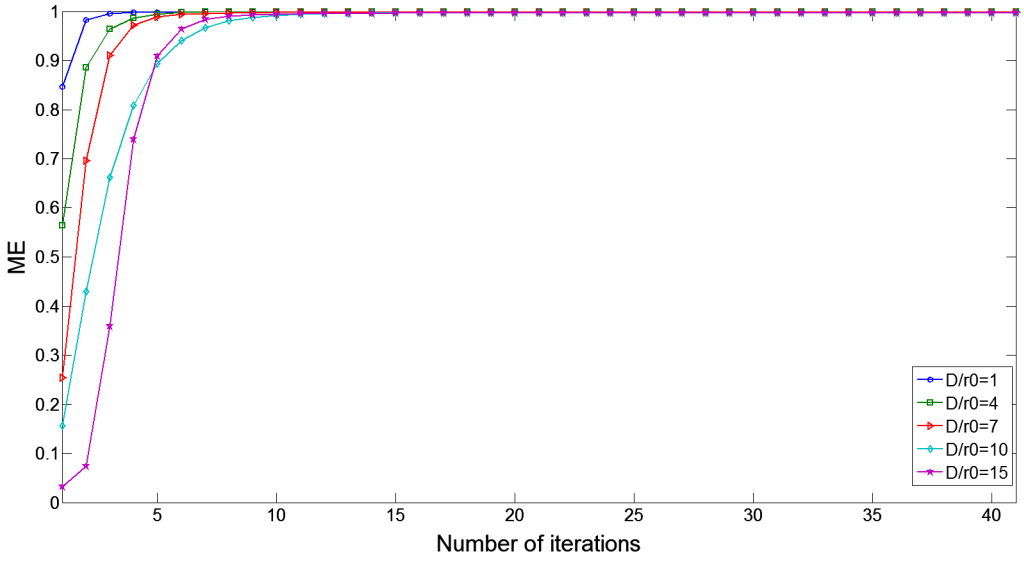

Fig. 5. The ME of heterodyne detection during the aberrations correction based-on the SPWFS.

formance of coherent FSO is given under different strength of turbulence with BPSK modulation. The wavelength is 632.8 nm, receiving antenna aperture is 8 mm, the gap between each micromirror is 5 μm, and the distinguishability of detector is 350 × 350 pixels.

4.1. The ME improvement by AO based-on SPWFS

According to the ME of homodyne detection, the ME of homodyne detection during the aberrations correction based-on SPWFS over different atmospheric turbulence strength is shown in Fig. 4.

As illustrated in Fig. 4, with the increase of D/r_0, the initial ME is dropped. After 13 iterations, the ME tend to stable as 0.95. The larger D/r_0, the lower initial ME is and the more iterations is needed. Similarly, the ME of heterodyne detection over different atmospheric turbulence strength is shown in Fig. 5.

As shown in Fig. 5, with the increase of D/r_0, the initial ME is dropped. After about 18 iterations, the ME tend to stable as about 0.97. Similarly, the larger D/r_0, the lower initial ME is and the more iterations is necessary.

4.2. The BER improvement by AO based-on SPWFS

According to Eqs. (23) and (24), it is shown that the BER of coherent FSO is related to the quantum efficiency, the number of photons and ME. We assume the quantum efficiency and the ME are 1. For the homodyne detection, the relationship between photons number and BER under different D/r_0 is shown in Fig. 6.

As illustrated in Fig. 6, for the coherent FSO under atmospheric turbulence, when $D/r_0 < 7$, N_p increase to 100, the BER can be decreased to below 10^{-9}. While, if $D/r_0 < 10$, we increase N_p to above 100, the BER cannot be decreased to below 10^{-9}. In a similar way, for the heterodyne detection, the relationship between N_p and BER under different D/r_0 is shown in Fig. 7.

As shown in Figs. 6 and 7, under different D/r_0, the relationship between N_p and the BER of the homodyne detection is similar to the heterodyne detection.

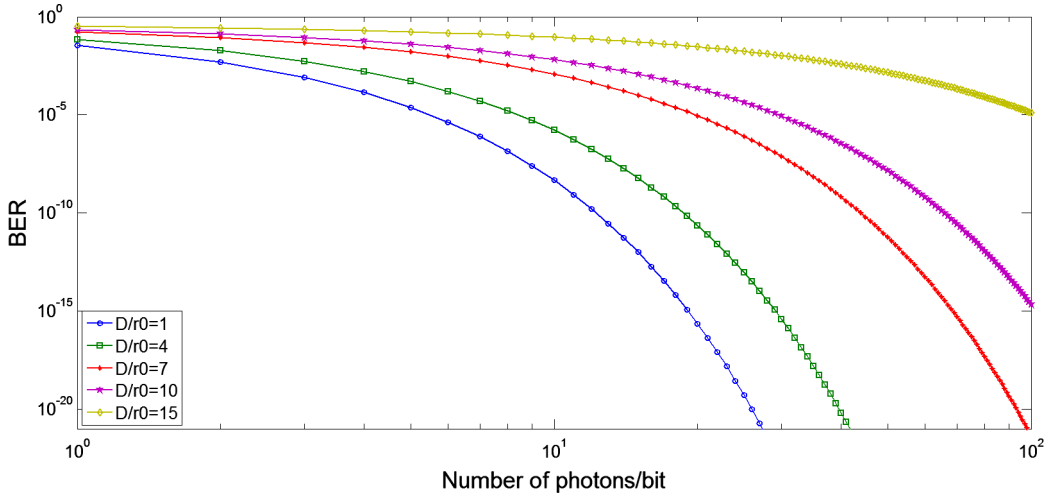

Fig. 6. The relationship between BER and the number of photons in the homodyne detection.

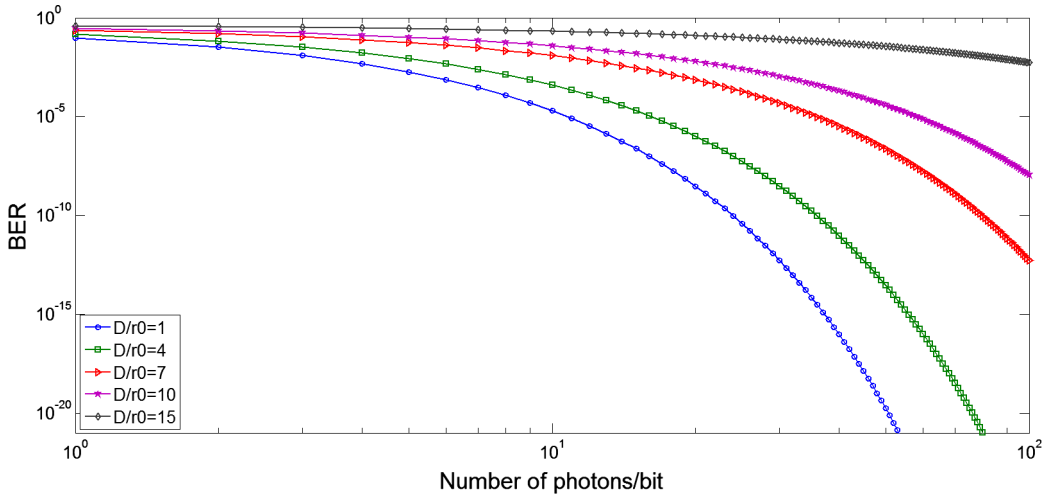

Fig. 7. The relationship between BER and the number of photons in the heterodyne detection.

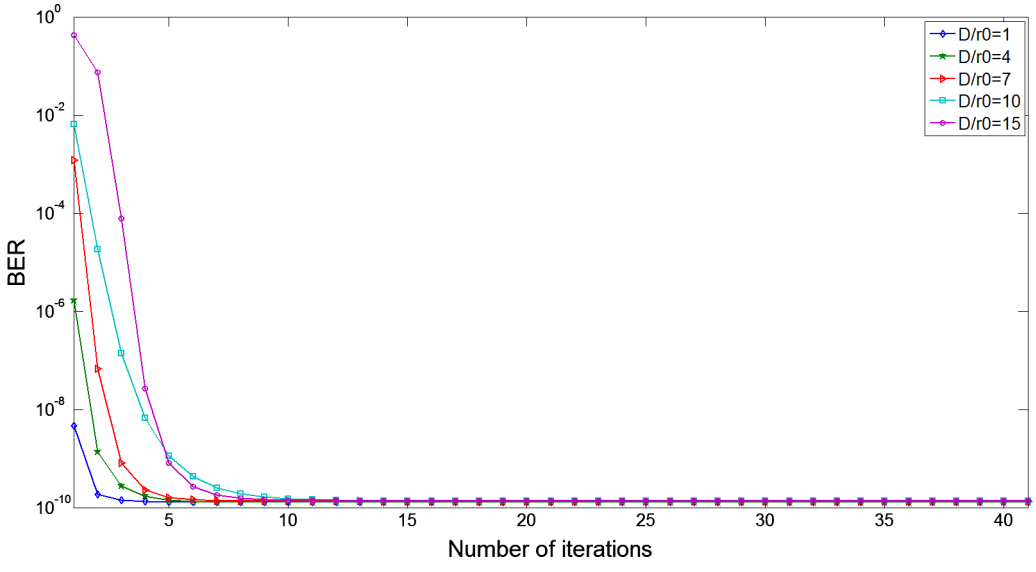

Fig. 8. The relationship between BER and the number iteration in homodyne detection.

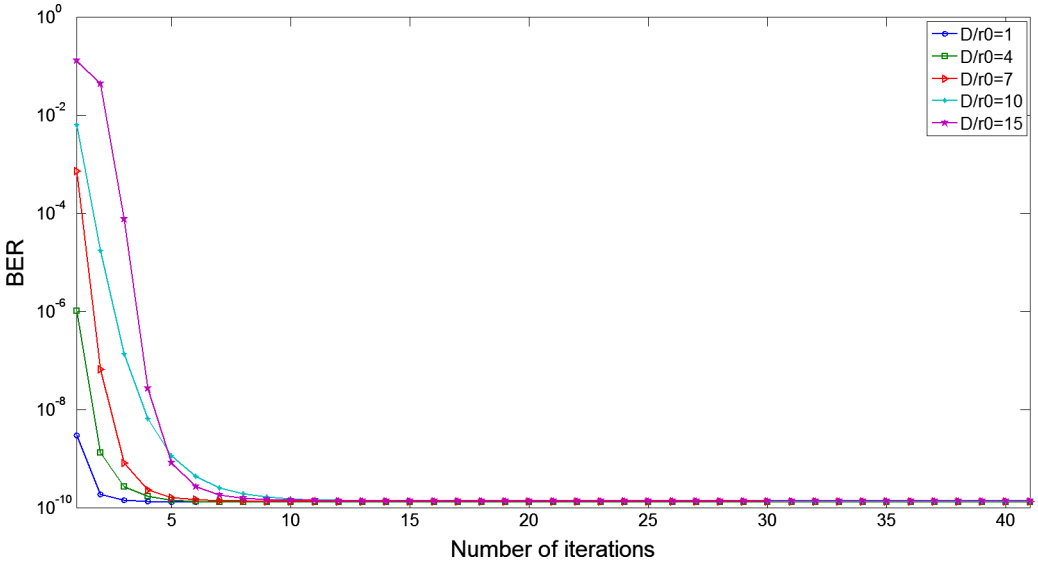

Fig. 9. The relationship between BER and the number of iteration in heterodyne detection.

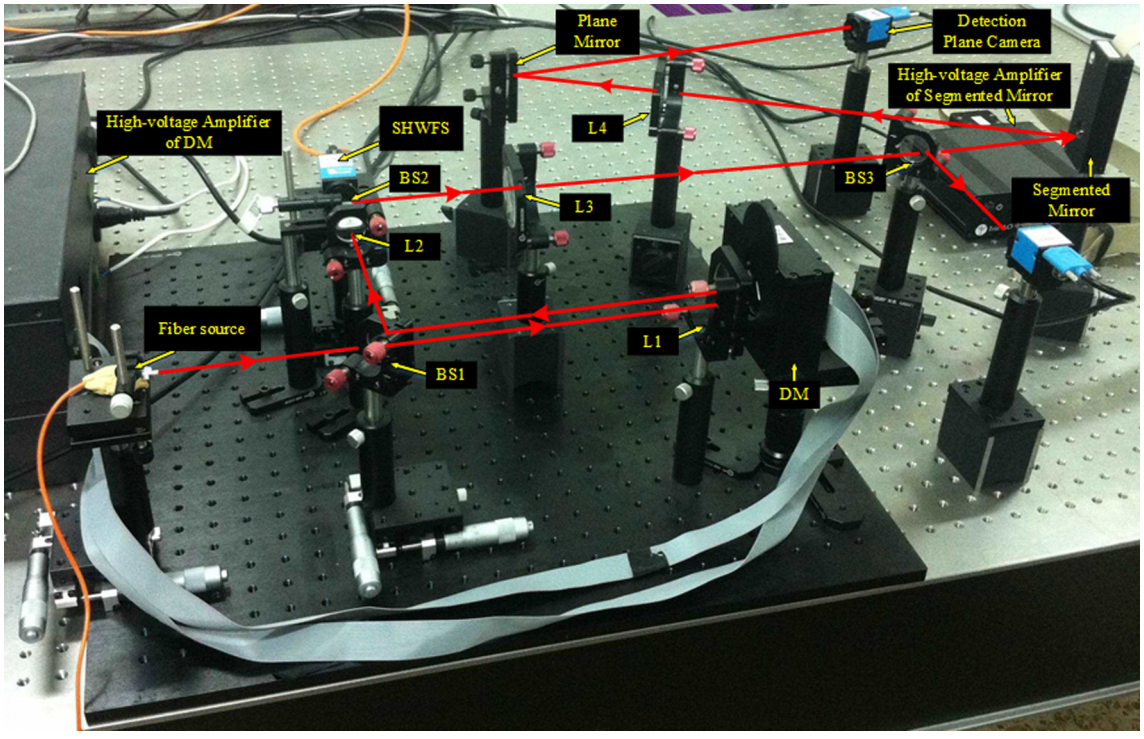

Fig. 10. The photo and the beam path.

In the following, the BER during aberrations correction of AO system based-on SPWFS is analyzed. We select $N_p = 10$ and $\eta = 1$. For the homodyne detection, the relationship between iterations and BER under different D/r_0 is shown in Fig. 8.

As shown in Fig. 8, with the increase of D/r_0, the system initial BER is increased. When $D/r_0 > 10$, the initial BER is above 10^{-2}; when $2 < D/r_0 < 10$, the initial BER is above 10^{-6}; if $D/r_0 = 1$, the initial BER is about 10^{-8}. After the correction of AO system based-on the SPWFS, the BER is stable about 10^{-10}. When the turbulence is increased, the more iterations is necessary. But after 11 iterations, it is convergence to a steady state. And after 6 iterations, the BER can decrease to 10^{-9}. Similarly, for the heterodyne detection, the

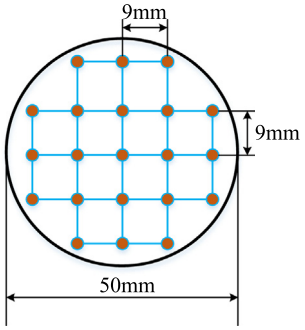

Fig. 11. The structure of DM.

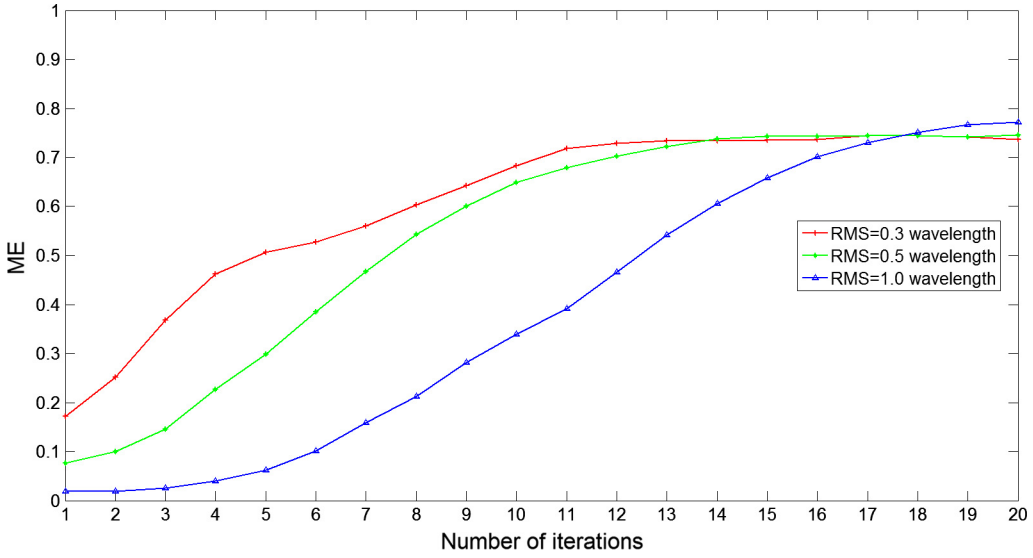

Fig. 12. The changing curve of ME during aberrations correction with different incident aberrations.

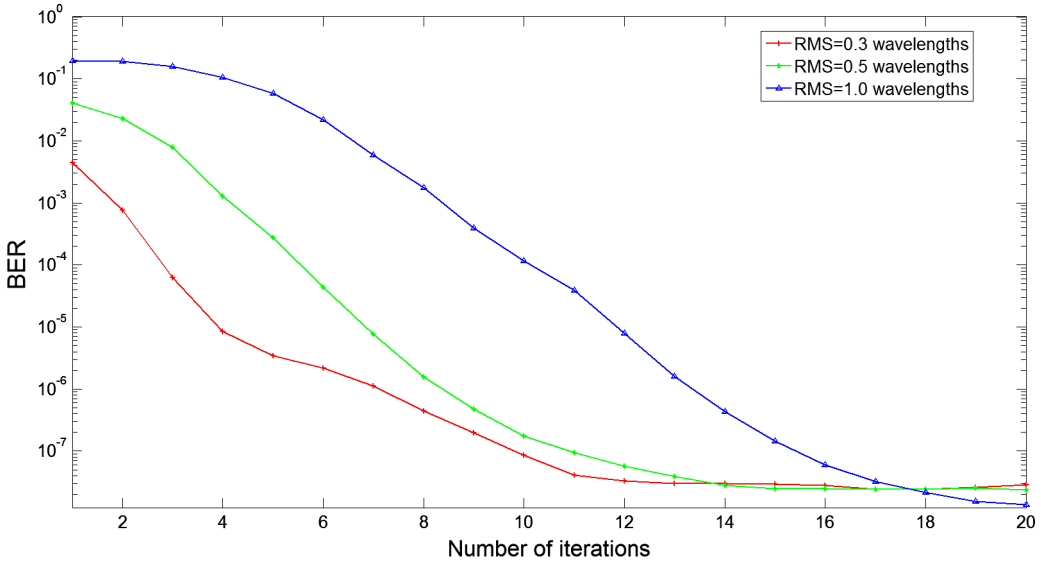

Fig. 13. The changing curve of BER during aberrations correction with different incident aberrations.

relationship between iterations and BER under different D/r_0 is shown in Fig. 9.

As shown in Fig. 9, except for the initial BER is lower than the homodyne detection, the trend of curve is basically the same with the homodyne detection. Similarly, the initial BER is increased with D/r_0 increases. After the correction of AO system based-on the SPWFS, the BER can reach to 10^{-10}. For the number of iterations, the BER can achieve the stable level of 10^{-10} after about 11 iterations, which is similar to homodyne detection. Likewise, the BER can reach to 10^{-9} after about 6 iterations.

5. Experimental analysis

In order to verify the performance of the coherent FSOC with AO based-on the SPWFS, an experimental system is designed, and the experimental data is used to analyze the ME and BER of homodyne detection. Similar to the AO based-on the PWFS, without any modulation holds many advantages in the closed-loop system [27]. The photo and the beam path are shown in Fig. 10.

In our experimental system, we select a 632.8 nm fiber source, and transform the experimental data to 1550 nm to be consistent with the communication wavelength [16]. The deformable mirror (DM) had a surface diameter of 50 mm, as well as 21 piezoelectric ceramic actuators which is arranged in 5×5 square with an actuator missing at each corner. The horizontal and vertical interval are 9 mm, which is shown in Fig. 11. The range of working voltage is from 0 V to 110 V. The range of measurement is from −5 μm to 5 μm. In our experiment, we label the position of actuator as 0 μm when the working voltage is 55 V. The focal length of L3 and L4 is 50 cm and 30 cm, respectively. The focal plane camera and detection plane camera are provided by Imaging Source Corporation with USB 3.0 interface. The highest resolution is 1280×960, and the fame rate is 60 fps, and the pixel size is 3.75 μm × 3.75 μm [25]. In addition, a SHWFS is adopted to monitor the state of the DM and provide a reference of the RMS value of the incident wavefront aberrations. The SHWFS has 37 subapertures in a 7×7 square, with three subapertures missing at each corner. Here, we assume $N_p = 10$ and $\eta = 1$.

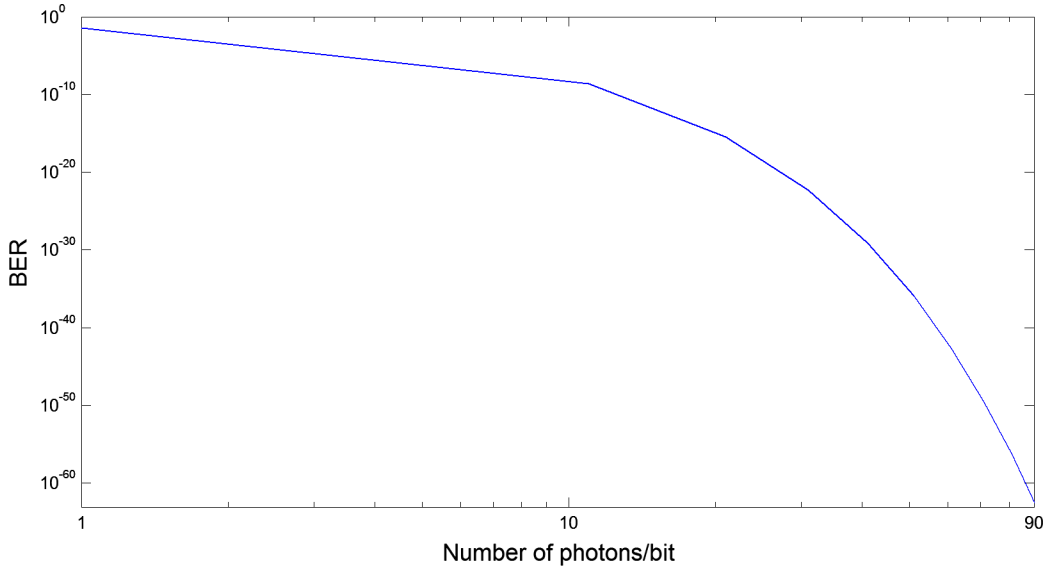

Fig. 14. The relationship between BER and the number of photons after correction when RMS is 1.0λ.

For the homodyne detection, the ME of the coherent FSOC is approximate to the Strehl ratio of the far field image of the laser beam [17]. Thus, when the RMS value of the incident wavefront aberrations is 0.3λ, 0.5λ and 1.0λ respectively (λ is the wavelength, here we select 1550 nm for the communication performance analysis), the changing curve of ME during the aberrations correction is shown in Fig. 12.

As shown in Fig. 12, when the RMS of the incident aberrations is 0.3λ, after about 13 iterations, the ME can increase from about 0.18 to about 0.7. And when the RMS of the incident aberrations is 0.5λ, after about 15 iterations, the ME can increase from about 0.08 to more than 0.7. Similarly, when the RMS of the incident aberrations is 1.0λ, after about 20 iterations, the ME can grow up from about 0.02 to more than 0.7.

According to Eq. (24), the changing curve of BER during the aberrations correction with different incident aberrations is shown in Fig. 13.

As shown in Fig. 13, after about 13 iterations, the BER can decrease from about 10^{-2} to below 10^{-7}, when the RMS value of the incident wavefront aberrations is 0.3λ. And after about 15 iterations, the BER can decrease from below 10^{-1} to below 10^{-7}, when the RMS value of the incident wavefront aberrations is 0.5λ. Similarly, after about 20 iterations, the BER can decrease from about 10^{-1} to nearly 10^{-8}, when the RMS value of the incident wavefront aberrations is 1.0λ.

According to the experimental results, we can see that the number of iterations is increasing with the increase of incident wavefront aberrations. However, the stable values of convergence are similar since the far-field focal spot is close to the diffraction limit (The ME is about 0.75 and the BER is below 10^{-7}).

After aberrations correction, the BER changing curve with different N_p when the incident wavefront aberrations is 1.0λ is shown in Fig. 14.

As shown in Fig. 14, with the increase of N_p, there will be a marked drop in BER. When $N_p > 12$, BER will be decrease below 10^{-9}.

6. Discussion and conclusion

Based on the previous study on the theory of the SPWFS, the SPWFS is first applied to the coherent FSOC with several advantages in this paper, such as with more flexible spatial resolution than the SHWFS, higher uniformity of sensitivity than PWFS and so on. The ME and BER are analyzed during the aberrations correction. Numeral simulation and experimental system are introduced to evaluate the performance of coherent FSOC. The results show that the ME can increase to more than 0.7 and the BER is able to decrease to below 10^{-7} after aberrations correction, under the condition of different incident wavefront aberrations. Thus, we believe that the AO based-on SPWFS can improve the performance of coherent FSOC.

Though the AO based-on SPWFS enhance the performance of coherent FSOC significantly, the BER is not able to achieve 10^{-9}. We consider the reason is that N_p is only selected as 10. As Fig. 14 shown, when $N_p > 12$, the BER will be decrease to below 10^{-9}.

In this paper, the incident wavefront aberrations are static which is produced by initial surface of the DM. The dynamic aberrations correction experiment will be tried in the future work. In addition, an experimental CFSOC system with an AO unit will be building and the ME and BER will be measuring by special instruments.

Acknowledgement

This work was supported by National 863 Plan Project (2013AA063903), National Natural Science Foundation of China (No. 61601195) and China Postdoctoral Science Foundation (2016M590255).

References

[1] A. García-Zambrana, R. Boluda-Ruiz, C. Castillo-Vázquez, B. Castillo-Vázquez, Transmit alternate laser selection with time diversity for FSO communications, Opt. Express 22 (2014) 23861–23874.
[2] Z. Jiankun, D. Shengli, Z. Huili, D. Anhong, Theoretical and experimental studies of polarization fluctuations over atmospheric turbulent channels for wireless optical communication systems, Opt. Express 22 (2014) 32482–32488.
[3] L. Wei, Y. Kainan, H. Danian, L. Xudong, W. Liang, L. Yaowen, Performance evaluation of coherent free space optical communications with a double-stage fast-steering-mirror adaptive optics system depending on the Greenwood frequency, Opt. Express 24 (2016) 13288–13302.
[4] P. Joaquin, Z. Stanislav, G. Zabih, P. Wasiu, Experimental characterization and mitigation of turbulence induced signal fades within an ad hoc FSO network, Opt. Express 22 (2014) 3208–3218.

[5] T.C. Farrell, Fast simulation of Strehl loss due to phase aberration for the sizing of adaptive optics in laser communications system design, Appl. Opt 53 (2014) 64–70.
[6] Y. Rahmat-Samii, A.C. Densmore, Technology trends and challenges of antennas for satellite communication systems, IEEE Trans. on Antennas and Propagation 03 (2014) 1–14.
[7] W. Liu, W. Shi, K. Yao, J. Cao, P. Wu, X. Chi, Fiber Coupling efficiency analysis of free space optical communication systems with holographic modal wavefront sensor, Opt. Laser Technol. 60 (2014) 116–123.
[8] J. Cao, X. Zhao, W. Liu, Y. Song, Stochastic parallel gradient descent laser beam control algorithm for atmospheric compensation in free space optical communication, OPTIK 125 (2014) 6142–6147.
[9] W. Liu, W. Shi, J. Cao, Y. Lv, S. Wang, J. Wang, X. Chi, Bit error rate analysis with real-time pointing errors correction in free space optical communication systems, OPTIK 125 (2014) 324–328.
[10] Y. Kainan, W. Jianli, L. Xinyue, L. Wei, Closed-loop adaptive optics system with a single liquid crystal spatial light modulator, Opt. Express 2014 (22) (2014) 17216–17226.
[11] A. Belmonte, A. Rodríguez, F. Dios, A. Comeón, Phase compensation considerations on coherent, free-space laser communications system, Proc. SPIE, 2007, vol. 6736, A-11.
[12] A. Belmonte, Influence of atmospheric phase compensation on optical heterodyne power measurements, Opt. Express 16 (2008) 6756–6767.
[13] L. Zuo, Y. Ren, A. Dang, G. Hong, Performance of coherent BPSK systems using phase compensation and diversity techniques, in: Proceedings of IEEE Conference on Global Telecommunications, 2010, 1–5.
[14] L. Zuo, A. Dang, Y. Ren, H. Guo, Performance of phase compensated coherent free space optical communications through non-Kolmogorov turbulence, Opt. Commun. 28 (2011) 41491–41495.
[15] M. Li, M. Cvijetic, Coherent free space optics communications over the maritime atmosphere with use of adaptive optics for beam wavefront correction, Appl. Opt. 54 (2015) 1453–1462.
[16] C. Liu, S. Chen, X. Li, H. Xian, Performance evaluation of adaptive optics for atmospheric coherent laser communications, Opt. Express 22 (2014) 15554–15563.
[17] C. Liu, M. Chen, S. Chen, H. Xian, Adaptive optics for the free-space coherent optical communications, Opt. Commun. 361 (2016) 21–24.
[18] H. Jian, D. Ke, L. Chao, Z. Peng, J. Dagang, Y. Zhoushi, Effectiveness of adaptive optics system in satellite-to-ground coherent optical communication, Opt. Express 22 (2014) 16000–16007.
[19] J. Huang, H. Mei, K. Deng, L. Kang, W. Zhu, Z. Yao, Signal to noise ratio of free space homodyne coherent optical communication after adaptive optics compensation, Opt. Commun. 356 (2015) 574–577.
[20] W. Liu, W. Shi, B. Wang, K. Yao, Y. Lv, J. Wang, Free space optical communication performance analysis with focal plane based wavefront measurement, Opt. Commun. 309 (2013) 212–220.
[21] R. Ragazzoni, Pupil plane wavefront sensing with an oscillating prism, J. Mod. Opt. 43 (1996) 289–293.
[22] S. Esposito, E. Pinna, A. Puglisi, A. Tozzi, P. Stefanini, Pyramid sensor for segmented mirror alignment, Opt. Lett. 30 (2005) 2572–2574.
[23] A. Wang, J. Yao, P. Cai, H. Ren, Design and fabrication of pyramid wavefront sensor, Opt. Eng. 49 (2010) 07401.
[24] Y. Kainan, W. Jianli, L. Xinyue, L. Hongwen, W. Minghao, C. Bochuan, Y. Shuhai, Pyramid wavefront sensor using a sequential operation method, Appl. Opt 54 (2015) 3894–3901.
[25] L. Chen, J. Wang, K. Yao, X. Liu, X. Lin, L. Wang, M. Wang, Experimental demonstration of sequential operation approach for three-sided pyramid wavefront sensor, IEEE Photon. J. 8 (2016).
[26] N. Roddier, Atmospheric wavefront simulation using Zernike polynomials, Opt. Eng. 29 (1990) 1174–1180.
[27] S. Wang, C. Rao, H. Xian, J. Zhang, J. Wang, Z. Liu, Laboratory demonstrations on a pyramid wavefront sensor without modulation for closed-loop adaptive optics system, Opt. Express 19 (2011) 8135–8150.